A chemorepellent inhibits local Ras activation to inhibit pseudopod formation to bias cell movement away from the chemorepellent

Sara A. Kirolos and Richard H. Gomer*
Department of Biology, Texas A&M University, College Station, TX 77843-3474

ABSTRACT **The ability of cells to sense chemical gradients is essential during development, morphogenesis, and immune responses. Although much is known about chemoattraction, chemorepulsion remains poorly understood. Proliferating *Dictyostelium* cells secrete a chemorepellent protein called AprA. AprA prevents pseudopod formation at the region of the cell closest to the source of AprA, causing the random movement of cells to be biased away from the AprA. Activation of Ras proteins in a localized sector of a cell cortex helps to induce pseudopod formation, and Ras proteins are needed for AprA chemorepulsion. Here we show that AprA locally inhibits Ras cortical activation through the G protein–coupled receptor GrlH, the G protein subunits Gβ and Gα8, Ras protein RasG, protein kinase B, the p21-activated kinase PakD, and the extracellular signal–regulated kinase Erk1. Diffusion calculations and experiments indicate that in a colony of cells, high extracellular concentrations of AprA in the center can globally inhibit Ras activation, while a gradient of AprA that naturally forms at the edge of the colony allows cells to activate Ras at sectors of the cell other than the sector of the cell closest to the center of the colony, effectively inducing both repulsion from the colony and cell differentiation. Together, these results suggest that a pathway that inhibits local Ras activation can mediate chemorepulsion.**

Monitoring Editor
Carole Parent
University of Michigan

Received: Oct 26, 2020
Revised: Oct 28, 2021
Accepted: Nov 9, 2021

INTRODUCTION

Chemotaxis, the movement of a cell toward or away from an external signal, is a fundamental process in developmental biology and immune function (Schwartz and Horwitz, 2006; Bagorda and Parent, 2008; King and Insall, 2009; Rappel and Loomis, 2009; Petri and Sanz, 2018; Thomas *et al.*, 2018). Work in the model eukaryote *Dictyostelium discoideum* has elucidated many aspects of chemoattraction, the movement of cells toward a signal. Like many motile eukaryotic cells, *Dictyostelium* can move by extending a pseudopod, allowing the pseudopod to adhere, and then contracting the trailing edge of the cell to push the cell forward (Devreotes and Zigmond, 1988; Uchida and Yumura, 2004; Ananthakrishnan and Ehrlicher, 2007; Cooper *et al.*, 2012; Eidi, 2017). During development, *Dictyostelium* cells aggregate using chemoattraction to cyclic adenosine monophosphate (cAMP) (Saran *et al.*, 2002; Garcia and Parent, 2008; De Palo *et al.*, 2017; Singer *et al.*, 2019). Five major pathways downstream of the cAR1 cAMP receptor, including target of rapamycin complex 2 (mTORC2), guanylyl cyclase, the mitogen-activated protein kinase (MAPK) cascade, phosphatidylinositol 3 kinase (PI3K)/phosphatidylinositol triphosphate (PIP3), and phospholipase A appear to act synergistically to promote the formation of new pseudopods on the side of cells closest to the source of the cAMP to drive chemoattraction (Kim *et al.*, 1998; Postma *et al.*, 2003; Stepanovic *et al.*, 2005; Chen *et al.*, 2007; Veltman *et al.*, 2008; Van Haastert, 2010; Bretschneider *et al.*, 2016; Nichols *et al.*, 2019).

This article was published online ahead of print in MBoC in Press (http://www.molbiolcell.org/cgi/doi/10.1091/mbc.E20-10-0656) on November 17, 2021.

*Address correspondence to: Richard H. Gomer (rgomer@tamu.edu).

Abbreviations used: ANOVA, analysis of variance; AprA, autocrine proliferation repressor protein A; ARP 2/3, actin related protein 2/3; cAMP, cyclic adenine monophosphate; cAR1, cyclic AMP receptor 1; DIC, differential interference contrast; DPPIV, dipeptidyl peptidase IV; ElmoE, engulfment and cell motility E; Erk, extracellular signal-regulated kinase; FMI, forward migration index; GDP, guanosine diphosphate; GefA, Ras guanine nucleotide exchange factor A; GFP, green fluorescent protein; GTP, guanosine triphosphate; MAPK, mitogen-activated protein kinase; mTOR, target of rapamycin; mTORC2, target of rapamycin complex 2; PakD, p21-activated kinase; PBS, phosphate buffer saline; PI3K, phosphoinositide-3-kinase; PIP3, phosphatidylinositol triphosphate; PKA, protein kinase A; PKB, protein kinase B; PlaA, phospholipase A; rAprA, recombinant AprA; Ras, rat sarcoma virus; RBD, Ras binding domain; SCAR, suppressor of cAR; SEM, standard error of the mean; WT, wildtype.

Chemorepulsion is the movement of cells away from a signal. Signals such as ephrin and slit cause repulsion of neuronal growth cones and dendritic spines (Hu, 1999; Nguyen-Ba-Charvet *et al.*, 1999; Havlioglu *et al.*, 2002; Goldberg *et al.*, 2013; Lisabeth *et al.*, 2013; Pilling *et al.*, 2019; Adhikari *et al.*, 2020). For amoeboid cells such as neutrophils, compared with chemoattraction, relatively little is known about chemorepulsion (Herlihy *et al.*, 2013, 2015, 2017; White *et al.*, 2018; Pilling *et al.*, 2019). We previously found an endogenous chemorepellent that is secreted by proliferating *Dictyostelium* cells called autocrine proliferation repressor protein A (AprA) (Phillips and Gomer, 2012) and has structural and functional similarity to human dipeptidyl peptidase IV (DPPIV) (Herlihy *et al.*, 2013, 2015, 2017; White *et al.*, 2018). In a colony of growing cells, the extracellular AprA concentration will be high in the colony and low outside the colony, creating a gradient. This AprA gradient causes cells at the edge of a colony to move away from the colony, possibly to find new sources of food (Phillips and Gomer, 2012).

Rather than inducing new pseudopods, AprA simply inhibits pseudopod formation at the region of the cell closest to the source of the AprA, causing the normal random cell motility to be biased away from the AprA source (Rijal *et al.*, 2019). Major proteins involved in the AprA-induced chemorepulsion pathway include the G protein–coupled receptor GrlH, the Gβ and Gα8 G protein subunits, protein kinase A, components of the mTOR2, phospholipase A, Erk1, PakD, and the Ras proteins RasC and RasG (Wu *et al.*, 1995; Bakthavatsalam *et al.*, 2009; Phillips and Gomer, 2014; Tang *et al.*, 2018; Rijal *et al.*, 2019). Unlike chemoattraction toward cAMP, the PI3K/Akt/protein kinase B and guanylyl cyclase pathways are not vital to induce biased movement away from AprA (Ma *et al.*, 1997; Kortholt *et al.*, 2011; Rijal *et al.*, 2019).

Some of the key regulators of the AprA-induced chemorepulsion pathway are Ras proteins (Rijal *et al.*, 2019). Ras proteins function as molecular switches that activate downstream pathways such as the PI3K/Akt/mTOR and the MAPK cascade to promote cytoskeletal rearrangement for cell polarization and motility (Kyriakis *et al.*, 1992; Suire *et al.*, 2006). Ras proteins also regulate processes such as proliferation, phagocytosis, and migration (Wennerberg *et al.*, 2005; Pal *et al.*, 2019). Ras proteins cycle between an active state, where the Ras is bound to guanosine triphosphate (GTP), and an inactive state, where the GTP on the Ras has been hydrolyzed to guanosine diphosphate (GDP) (Bourne *et al.*, 1991). Ras activation can be regulated by proteins such as Rho GTPases (Wang *et al.*, 2013) and Erk1/2 through negative feedback loops (Lake *et al.*, 2016). In *Dictyostelium*, the Ras proteins RasC and RasG are both needed for chemoattraction to cAMP (Kae *et al.*, 2004; Sasaki *et al.*, 2004; Bolourani *et al.*, 2006; Kortholt *et al.*, 2011). We previously found that *rasC*$^-$ and *rasG*$^-$ null mutants are repelled in an AprA gradient, but *rasC*$^-$/*rasG*$^-$ double mutants fail to repel (Rijal *et al.*, 2019), suggesting that RasC and RasG have overlapping functions needed for chemorepulsion (Artemenko *et al.*, 2014).

In a cAMP gradient, to initiate cell polarity and pseudopod formation, Ras activation has three phases (Kortholt *et al.*, 2013). The first phase is Ras activation at the entire boundary of the cell (Kortholt *et al.*, 2013). The second and third phases are symmetry breaking in which Ras activation is localized at the leading edge of the cell toward the chemoattractant (Kortholt *et al.*, 2013). When Ras-GTP is localized at the leading edge, downstream pathways such as TORC2-PKB and key proteins such as WAVE/SCAR and Arp2/3 complex are activated to induce actin filament formation and pseudopod formation (Ridley, 2001; Charest *et al.*, 2010). Ras activation at the leading edge of a *Dictyostelium* cell in a cAMP gradient recruits PI3 kinases to the leading edge of the cell (Heid *et al.*, 2005; Bosgraaf and Van Haastert, 2009). The recruited PI3 kinases increase levels of PIP3 at the inner face of the plasma membrane at the leading edge of the cell, and this leads to actin polymerization and pseudopod formation (Sasaki *et al.*, 2004; Janetopoulos and Firtel, 2008). Conversely, the Ras GTPase-activating proteins RasGAP2 and RasGAP3 as well as phosphatidylinositol bisphosphate (PIP2) show higher concentrations at the trailing edge of the cell and render Ras in an inactive state (Ras-GDP), reducing actin polymerization (Li *et al.*, 2018). The activation of Ras at the leading edge of the cell thus causes directed migration of amoeboid cells (Cai *et al.*, 2010; Rappel and Edelstein-Keshet, 2017; Cheng *et al.*, 2020).

Because AprA inhibits pseudopod formation at the region of a cell closest to the source of the AprA, and because active Ras is involved in pseudopod formation and is required for AprA-induced chemorepulsion, in this report we examined the effect of AprA on Ras activation. We find that AprA inhibits local Ras activation at the side of a cell closest to the source of the AprA using a pathway involving GrlH, Gβ, Gα8, PKB, PakD, Erk1, and RasG, helping to explain how AprA inhibits pseudopod formation.

RESULTS

A gradient of AprA causes a redistribution of GTP-Ras

We have previously shown that, compared with cells in buffer, neutrophils exposed to a DPPIV gradient and *Dictyostelium* cells exposed to a recombinant AprA (rAprA) gradient in an Insall chamber showed a biased movement away from the chemorepellent (Phillips and Gomer, 2012; Herlihy *et al.*, 2013) (Supplemental Videos 1 and 2). For unknown reasons, ~17% of both neutrophils and *Dictyostelium* cells showed movement toward the source of chemorepellent (Phillips and Gomer, 2012; Herlihy *et al.*, 2013) (Supplemental Videos 1 and 2). To image cells in a gradient of AprA in an eight-well slide, we cultured cells in eight-well slides and added rAprA to the corner of the well. Diffusion calculations indicated that AprA should diffuse more slowly than a small-molecule dye (Supplemental Figure 1A). When dye was added to the corner of the well and then imaged, the dye spread across the well faster than expected for diffusion, indicating that convection in the well plays a significant role in causing the dye to spread across the well (Supplemental Figure 1, A and B). Because convection will move a soluble protein approximately as much as a dye, the data in Supplemental Figure 1 indicate that there will be a gradient of rAprA in the center of the well at 20 min after adding rAprA to the corner of the well. Raf1-RBD-GFP is a chimeric protein containing the Ras-binding domain of Raf1 fused to the fluorescent protein GFP and preferentially binds to GTP-Ras compared with GDP-Ras, allowing localization of active Ras (Sasaki *et al.*, 2004). In a cAMP gradient, in starved wild-type cells expressing Raf1-RBD-GFP, as previously observed (Sasaki *et al.*, 2004; Zhang *et al.*, 2008; Kortholt *et al.*, 2013), Raf1-RBD-GFP was localized at the front of the cell, the region of the cell that is toward the source of cAMP (Figure 1, A and B). We previously found that cells at high density accumulate 300 ng/ml extracellular AprA (Choe *et al.*, 2009). To test the hypothesis that AprA inhibits pseudopod formation by inhibiting Ras activation, Ax2 cells expressing Raf1-RBD-GFP were exposed to a gradient of buffer or buffer with 300 ng/ml rAprA (Choe *et al.*, 2009) for 20 min (conditions that cause no chemorepulsion or chemorepulsion, respectively) (Phillips and Gomer, 2012) and then imaged (Figure 1C). As previously observed in *Dictyostelium* cells (Sasaki *et al.*, 2004; Kortholt and Van Haastert, 2008; Rijal *et al.*, 2019), Raf1-RBD-GFP localized at part of but not the entire circumference near the cortex of cells (Figure 1C). In the absence of a gradient, 50 ± 4% of the cells had

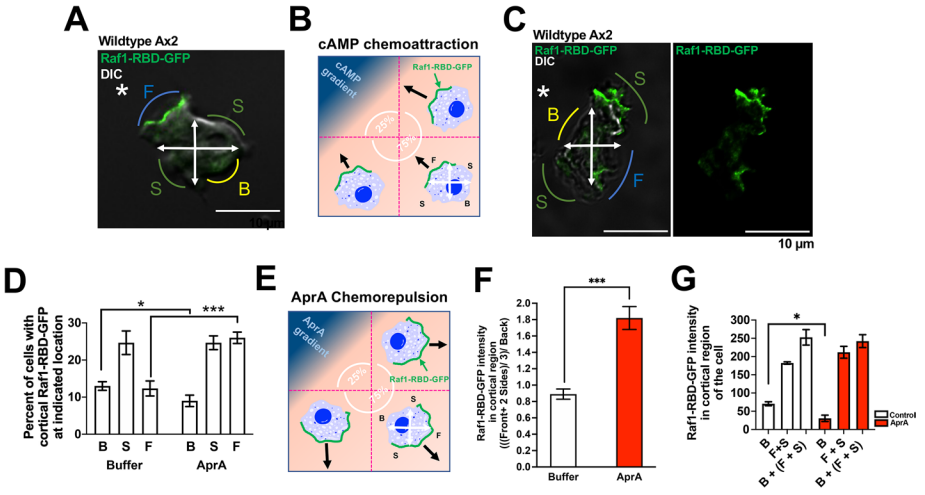

FIGURE 1: AprA redistributes Ras cortical activation to the region of the cell away from a source of AprA. (A) Live image of a wild-type Ax2 cell transformed with Raf1-RBD-GFP construct in a cAMP gradient. * indicates the direction from the cell where cAMP was added. F indicates the front of the cell or region of the cell nearest to cAMP. S indicates the sides of the cells. B indicates the back of the cell or the region of the cell away from the gradient. The white arrows separate the different regions of the cell. Image shows combined fluorescence and DIC. Bar is 10 µm. Image is representative of cells from three independent experiments. (B) Schematic of wild-type Ax2 cells in a chamber with cAMP gradient at the top left corner of the well. The white arrows indicate the different regions of the cell. The green outline on the cells indicates where the majority of the Raf1-RBD-GFP is distributed. (C) Live image of a wild-type Ax2 cell transformed with Raf1-RBD-GFP construct in a recombinant AprA (rAprA) gradient. * indicates the direction from the cell where rAprA was added. F indicates the front of the cell or region of the cell farthest from rAprA. S indicates the sides of the cells. B indicates the back of the cell or the region of the cell nearest to the gradient. The white arrows separate the different regions of the cell. Image shows combined fluorescence and DIC. Bar is 10 µm. Image is representative of cells from five independent experiments. (D) Cells were imaged and scored for Ras localization. Graph shows the percent of cells with cortical Raf1-RBD-GFP at the back (B), at one or both sides (S), or the front (F) of the cell. Values are mean ± SEM of the averages from five independent experiments, with at least 30 randomly chosen cells examined in each condition in each experiment. *$p < 0.05$, ***$p < 0.001$ (two-way ANOVA, Holm–Šídák's test). (E) Schematic of wild-type Ax2 cells in a chamber with rAprA gradient at the top left corner of the well. The white arrows separate the different regions of the cell. The green outline on the cells indicates where most of the Raf1-RBD-GFP is distributed. (F) Cells were imaged and scored for the difference in Raf1-RBD-GFP intensity at the front and sides of the cell and at the back of the cell. Graph shows the ratio of ([Raf1-RBD-GFP intensity at the front and sides of the cells combined]/3) to (Raf1-RBD-GFP intensity at the back of the cell). (G) Graph shows the Raf1-RBD-GFP intensity (in arbitrary units) at the back (B), front and sides (F + S), and entire cortical region of the cell (B + (F + S)). For F and G, values are mean ± SEM of the averages from four independent experiments, with at least 90 randomly chosen cells examined for each point in each experiment. *$p < 0.05$, ***$p < 0.001$ (unpaired *t* tests, Welch's correction).

discernible Raf1-RBD-GFP localization to some part of the cell cortex, while a rAprA gradient caused this to increase to 60 ± 3% (mean ± SEM, $n = 3$ with ~85 cells assayed in each experiment, $p = 0.02$, *t* test) (Figure 1D). Compared with control, a decreased percentage of cells in an AprA gradient showed detectable Raf1-RBD-GFP in the cortex at the region toward the source of the rAprA (here defined as the back of the cell) and an increased percentage of cells showed detectable Raf1-RBD-GFP in the cortex at the region away from the source of the rAprA (here defined as the front of the cell) (Figure 1D and Supplemental Videos 3 and 4). For the videos, we observed that due to the high autofluorescence of the HL5 medium, each fluorescence image of cells to detect Raf1-RBD-GFP required a high exposure to the excitation light and repeated fluorescence imaging of cells caused the Raf1-RBD-GFP to photobleach. The videos were thus done with cells in a 1:1 mixture of HL5 and SIH (a synthetic medium with considerably less autofluorescence). Compared with cells in a buffer gradient, cells in a rAprA gradient showed less Raf1-RBD-GFP intensity at the back of the cell and similar levels at the front and sides of the cells (Figure 1, E–G). These data suggest that an AprA gradient inhibits Ras activation at the back of a cell.

A uniform concentration of AprA decreases Ras activation in the cortex

To determine the time needed for rAprA to alter Ras activation, Ax2 wild type and cells lacking the AprA receptor GrlH (*grlH*$^-$ cells) expressing Raf1-RBD-GFP were exposed to a uniform concentration of 300 ng/ml rAprA or buffer and live images were taken (Figure 2A and Supplemental Figure 2A). *Dictyostelium* cells show chemorepulsion in an AprA gradient after 20 min (Phillips and Gomer, 2012), and 5- and 20-min exposures of cells to rAprA increase levels of Ras at the cell cortex (Rijal *et al.*, 2019). We observed a similar effect at 5, 10, and 20 min (Figure 2B), but rAprA then reduced levels of Raf1-RBD-GFP cortical localization after 30 min (Figure 2, A and B). rAprA did not decrease levels of active Ras at the cortex in cells lacking the AprA receptor GrlH (Figure 2C and Supplemental Figure 2A). A pan-specific anti-Ras antibody raised against a sequence present in all known *Dictyostelium* Ras proteins showed similar levels of Ras in Ax2, *rasG*$^-$, *rasC*$^-$, *rasG*$^-$/*C*$^-$, and *rasD*$^-$ cells, indicating that the antibody recognizes one or more Ras proteins in addition to RasG, RasC, and RasD (Supplemental Figure 3). Western blots of whole cell lysates stained with the anti-Ras antibody indicated that compared with the addition of buffer, the addition of rAprA to cells caused no significant change of total Ras levels up to 60 min of AprA treatment (Supplemental Figure 2, B and C). Cells exposed to 150 ng/ml or lower concentrations of rAprA for 6 h also had no significant change in total Ras levels, whereas at 6 h, 185 ng/ml or higher concentrations of rAprA decreased Ras levels (Supplemental Figure 2D). To examine levels of GTP-bound Ras, cells were lysed and incubated with beads coated with GST-tagged Raf1-RBD protein, which preferentially binds GTP-bound Ras (Rijal *et al.*, 2019). Western blots of material bound to the beads stained with an antibody that detects the Ras antigen indicated that rAprA decreased levels of active Ras after 30 min in Ax2 cells (Figure 3). Similar to Ax2 cells, cells lacking endogenous AprA (*aprA*$^-$ cells) expressing Raf1-RBD-GFP showed slightly increased cortical Raf1-RBD-GFP localization at 10 and 20 min and decreased cortical localization after 30 min in response to rAprA (Supplemental Figure 4A). The *aprA*$^-$ cells also showed decreased Ras activation in response to rAprA in pull-down assays at and after 30 min (Supplemental Figure 4B).

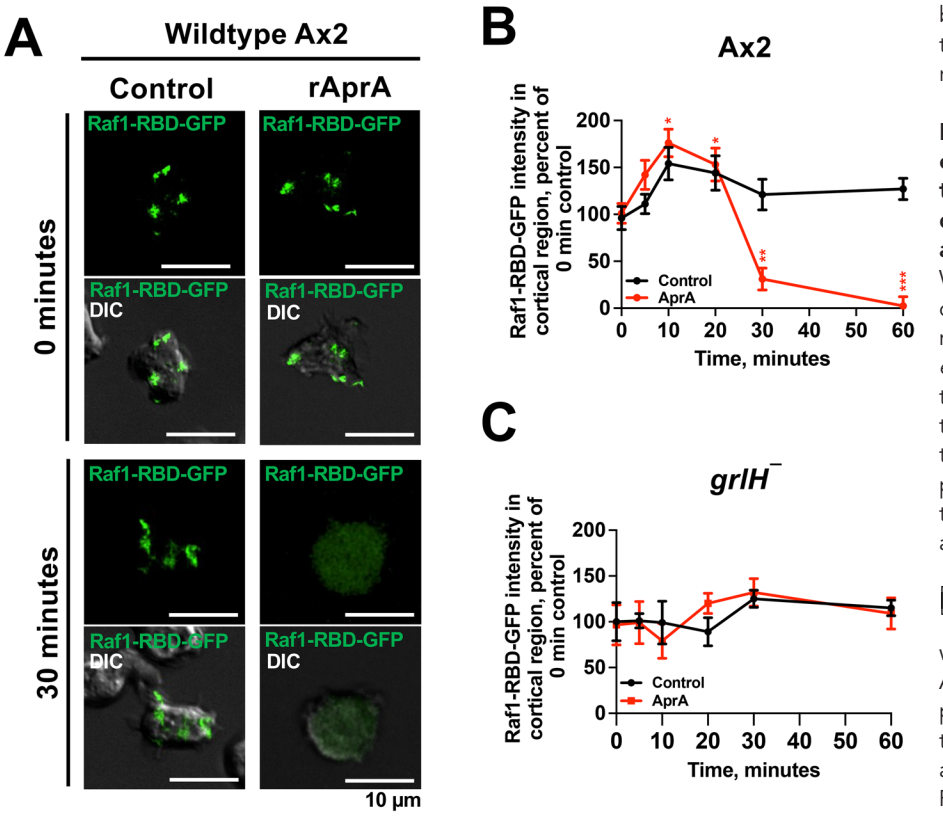

FIGURE 2: AprA inhibition of Ras cortical activation is time dependent, and rAprA does not inhibit Ras cortical activation in *grlH*⁻ cells. (A, B) Live imaging of wild-type Ax2 cells expressing Raf1-RBD-GFP in a uniform concentration of rAprA. (A) Image shows combined fluorescence and DIC. Bar is 10 μm. Image is representative of cells from five independent experiments. (B) Cells were imaged, and the graph shows the Raf1-RBD-GFP intensity at the cortical region of the cells, normalized to the 0-min control. (C) *grlH*⁻ cells expressing Raf1-RBD-GFP were incubated in 0 (control) or 300 ng/ml rAprA and then imaged at the indicated times. The Graph shows the Raf1-RBD-GFP intensity at the cortical region of the cells, normalized to the 0-min control. For B and C, values are mean ± SEM of the averages from three independent experiments, with at least 40 randomly chosen cells examined in each condition in each experiment. *$p < 0.05$, **$p < 0.01$, ***$p < 0.001$ compared with 0 min (unpaired *t* tests, Welch's correction).

At 60 min, AprA concentrations up to 80 ng/ml did not significantly decrease levels of Raf1-RBD-GFP at the cortex, while 115 ng/ml and higher did decrease levels of Raf1-RBD-GFP at the cortex (Figure 4, A and B). To determine whether removing rAprA can restore Ras activation at the membrane, cells expressing Raf1-RBD-GFP were incubated with 300 ng/ml rAprA or buffer in HL5 for 60 min, and the medium was then replaced with fresh HL5. Live cell images were then taken. We previously observed that a uniform concentration of 2 μg/ml of rAprA had no significant effect on motility (Phillips and Gomer, 2012). However, in agreement with the idea that AprA inhibits pseudopod formation (Rijal *et al.*, 2019) compared with cells that were not exposed to rAprA (Supplemental Video 5), 300 ng/ml rAprA caused the cells to round up and decrease their speed (Figure 5, A–C, and Supplemental Video 6). When the medium with rAprA was replaced with fresh HL5, the cells regained their amoeboid phenotype, and cortical Ras activation increased after 30 min in fresh media (Figure 5, A and D), indicating that AprA does not permanently inhibit Ras activation at the cortex. Together, these results suggest that a uniform concentration of AprA decreases cortical Ras activation and motility after 30 min, that there appears to be a threshold for this effect, that this requires GrlH but does not require cells to be expressing their own AprA, and that the effect can be reversed by removing AprA.

Diffusion calculations predict that endogenous AprA forms a gradient at the edge of a colony and can differentially affect cells at the center and edge of the colony

We previously predicted that in a colony of cells secreting AprA, a gradient of AprA might form at the edge of the colony (Rijal *et al.*, 2019). To calculate the local concentration of AprA at different places in an actual colony of cells, we first need to know the extracellular accumulation rate of AprA per cell per minute in a colony (ϕ; the secretion rate if there is no breakdown). A first approximation would be to use

$$[\text{AprA}] = N\phi\tau$$

where [AprA] is the amount of extracellular AprA at time τ, with cells washed and resuspended in fresh medium at time 0, and N is the cell density. However, the cells proliferate during this time, so N is not constant. For log-phase cells, with N_0 the initial cell density, the cell density $N(t)$ will be at time t

$$N(t) = N_0 e^{kt} \qquad (1)$$

Assuming no breakdown of AprA, the change in the extracellular AprA concentration at time t will be

$$d[\text{AprA}]/dt = N(t)\phi$$

The extracellular AprA concentration will then be at time τ

$$[\text{AprA}] = \int_0^\tau N(t)\phi \; dt = N_0\phi\int_0^\tau e^{kt}\, dt = \frac{N_0\phi}{k}\; e^{k\tau} - \frac{N_0\phi}{k}e^0$$

yielding

$$\phi = \frac{[\text{AprA}]k}{N_0\left(e^{k\tau}-1\right)} \qquad (2)$$

For the Ax2 cells and media used during these experiments, we observed that cells would proliferate by a factor of 3.5 ± 1.3 (mean ± SEM, $n = 5$) over 24 h, and from Eq. 1 we find that the mean $k = 8.7 \times 10^{-4}$/min. We then made colonies of cells in eight-well slides and measured the extracellular AprA. From Figure 6, a colony of $N_0 = 4 \times 10^5$ Ax2 cells accumulates 4.0 ng ± 0.8 ng of AprA in 6 h. From Eq. 2 we then find that the mean $\phi = 2.4 \times 10^{-8}$ ng AprA per cell per minute, in approximate agreement with the 2.6×10^{-8} ng AprA per cell per minute we previously measured for cells in shaking culture (Choe *et al.*, 2009). For cells on glass or plastic in submerged culture, the local concentration C of AprA at a distance x from a cell secreting AprA will be

$$C = 2\phi\left(\frac{1}{2\sqrt{\pi D}}\right)^3 \int_0^\tau t^{-\frac{3}{2}} e^{-\left(\frac{x^2}{4Dt}\right)} dt \qquad (3)$$

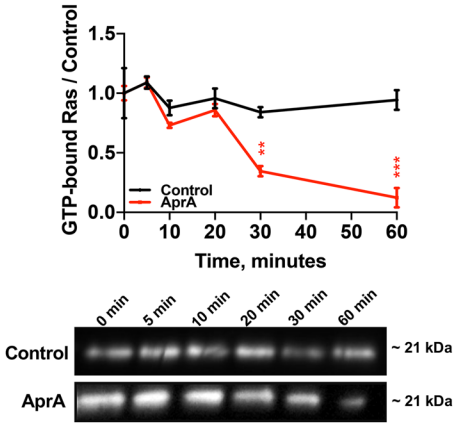

FIGURE 3: AprA inhibition of Ras cortical activation is time dependent. Ax2 cells were incubated with or without 300 ng/ml rAprA for the indicated times, and an aliquot of the samples was used for a Coomassie-stained gel. The remainder of the samples were used for Raf1-RBD affinity bead pull downs. These were electrophoresed on SDS–polyacrylamide gels, and Western blots were stained with an anti-Ras antibody (bottom figure). Band intensities were normalized to the corresponding Coomassie gel scans and total Ras. Graph shows the levels of GTP-bound Ras normalized to the 0-min control. Values are mean ± SEM of three independent experiments. $^{**}p < 0.01$, $^{***}p < 0.001$ compared with the 0-min control (unpaired *t* tests, Welch's correction).

(Yuen and Gomer, 1994), where *D* is the diffusion coefficient of the AprA. Extracellular AprA is in a 150 kDa complex with the protein CfaD (Bakthavatsalam *et al.*, 2008), and the diffusion coefficient of a protein of this size is ~5.0×10^{-7} cm^2/s (Bakthavatsalam *et al.*, 2008). This integral cannot be solved in closed form but can be converted to an infinite series (Yuen and Gomer, 1994). Although in the diffusion calculations one can correct for the presence of receptors on the cell surface binding to a secreted ligand, effectively decreasing the free ligand concentration (Yuen and Gomer, 1994), the data from Figure 6 show the free AprA from a colony of cells after some AprA has bound to cells, and thus to a first approximation can be used in the calculations for the free AprA in a colony of cells after some AprA has bound to cells. Equation 3 is for cells in an infinitely thick layer of medium. The colonies of cells were in 200 µl of medium in a 0.9×0.7 cm well, yielding an approximate thickness of 0.3 cm of medium over the colony. Figure 7A shows the calculated concentration of AprA after 6 h at different distances from a single cell continuously secreting AprA. This indicates that the concentration of AprA at 0.3 cm from the cell is 1.4×10^{-4} relative to the concentration immediately adjacent to the cell, indicating that the calculations for an infinitely thick layer of liquid above the cell will be a good approximation to what is happening in the well. As described in Gomer (2019), we can then calculate the concentration of AprA at different distances from the center of a colony of cells, summing the contribution from each cell at each distance from the colony center. Because the cells are proliferating, we corrected for cell proliferation by increasing the number of cells and the size of the colony every hour in the calculation. A colony of 4×10^5 cells, from observations, had an initial radius of 0.18 cm and after 6 h a radius of 0.21 cm; dividing the cell number by πr^2 indicated that the local surface density of cells remained constant. In colonies of 2×10^5 cells or fewer, from the center to the edge of the colony (vertical dotted line in Figure 7B), the predicted AprA concentration is below the 185 ng/ml threshold (horizontal dotted line in Figure 7B), where AprA decreases the levels of the antigen(s) recognized by the anti-Ras antibody. In a colony of 4×10^5 cells, the calculations predict that cells in the center will be exposed to AprA concentrations greater than 185 ng/ml, while an annulus of cells near the edge of the colony will be exposed to AprA concentrations below 185 ng/ml. The calculations also predicted that a smaller annulus would have AprA concentrations below the 115 ng/ml threshold (dashed line in Figure 7B), where AprA inhibits Ras cortical localization (Figure 4B). The calculations then predicted that cells from the center to the edge in colonies with 8×10^5 cells would be exposed to AprA concentrations above 185 ng/ml, thereby decreasing levels of the Ras antigen(s).

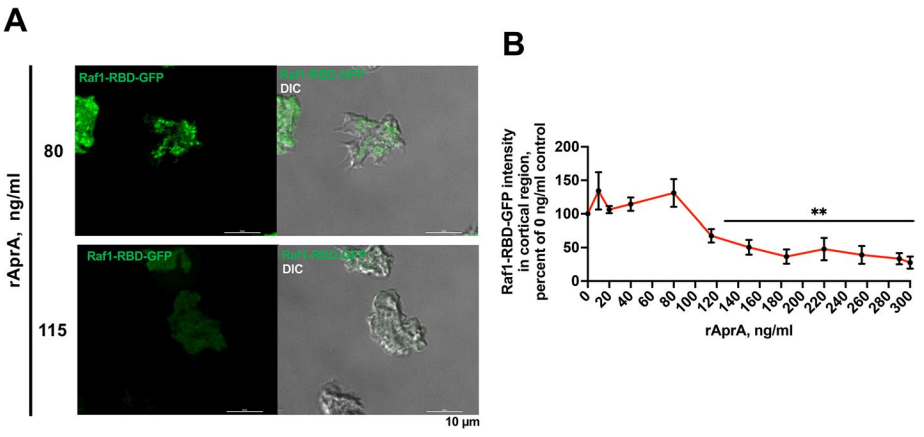

FIGURE 4: AprA inhibition of Ras cortical activation is concentration dependent. (A) Ax2 cells expressing Raf1-RBD-GFP were incubated with the indicated concentrations of rAprA for 60 min and then imaged. Image pairs are fluorescence at left and combined fluorescence and DIC at right. Bars are 10 µm. Images are representative of three independent experiments. (B) Graph shows Raf1-RBD-GFP (green) fluorescence intensity at the cortical region of cells, normalized to the 0 ng/ml rAprA control. Values are mean ± SEM of the averages from three independent experiments, with at least 40 randomly chosen cells examined for each point in each experiment. $^{**}p < 0.01$ compared with the 0 ng/ml rAprA control (unpaired t tests, Welch's correction).

The predicted AprA gradient at the edge of a colony affects Ras activation

Figure 7B predicts that for 4×10^5 cell colonies with initial radii of 0.18 cm, at 6 h there should be an endogenous gradient of AprA. As with cells in a rAprA gradient in a gradient chamber, in cells at the margin of these colonies, levels of cortical Raf1-RBD-GFP were decreased at the cortical region of the cell closest to the center of a colony compared with the cortical region of the cell away from the center of the colony (Figure 8, A, C, and E). This effect was observed for both fixed cells (Figure 8A) and live cells (Figure 8C). Figure 7B also predicts that for 4×10^5 cell colonies with initial radii of 0.18 cm, at 6 h there should be sufficient AprA near the center of the colony to inhibit Ras activation at the cell cortex, and we observed that this was indeed the case in fixed and live colonies (Figure 8, A, C, and F). For unknown reasons, whereas live cells at the center of the colony showed levels of total

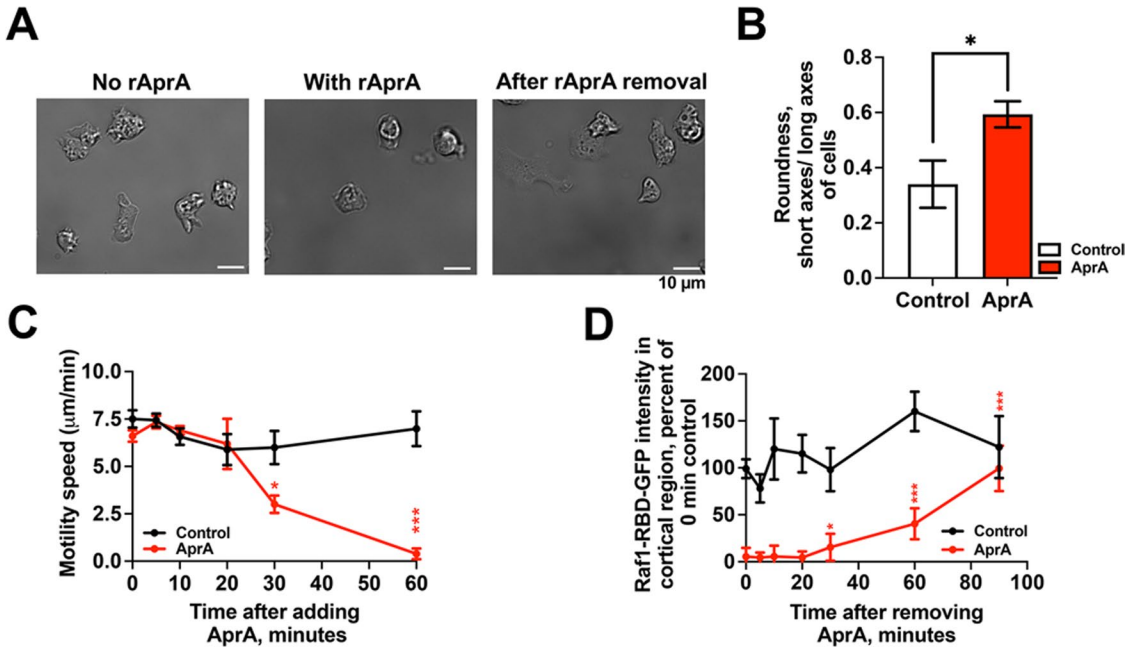

FIGURE 5: AprA removal can restore amoeboid phenotype and Ras activation at the cortex. (A) Wild-type Ax2 cells expressing Raf1-RBD-GFP (green) were incubated with or without 300 ng/ml rAprA in HL5 for 60 min, and the medium was then replaced with fresh HL5. DIC images of live cells before adding rAprA (left), at 60 min after adding rAprA (center), and at 90 min after removing rAprA (right). Images are representative of three independent experiments. Bars are 10 µm. (B) Roundness of cells exposed to rAprA for 60 min was determined by measuring the ratio of the short and long axes of the cell (short/long). (C) Graph shows motility speed, defined as the total path distance traveled divided by the time elapsed determined by measuring the position of a cell every 15 s for 30 min after adding rAprA. (D) Ax2 cells were incubated with or without (Control) rAprA for 1 h, and the medium was then replaced with fresh HL5. Cells were imaged at the indicated times after removing rAprA. Graph shows the Raf1-RBD-GFP (green) intensity at the cortical region of the cell, normalized to the 0-min control. Values are mean ± SEM of the averages from three independent experiments, with at least 40 randomly chosen cells examined for each point in each experiment. *$p < 0.05$, ***$p < 0.001$ compared with the 0-min preincubated with rAprA control (unpaired *t* tests, Welch's correction).

Raf1-RBD-GFP similar to those of the cells at the edge of a colony (Figure 8, C and D), the Raf1-RBD-GFP levels decreased in fixed cells at the center of a colony compared with cells at the edge of a colony (Figure 8, A and B). In low-power images of fixed colonies, this resulted in a ring of Raf1-RBD-GFP staining (Figure 8G). Because levels of AprA above 185 ng/ml decrease levels of the antigen detected by the anti-Ras antibody after 6 h (Supplemental Figure 2D), in agreement with Figure 7B, a ring of the antibody that binds to a Ras antigen was observed in 4×10^5 cell colonies (Supplemental Figure 5). In agreement with the prediction that colonies with the same size but a lower density of cells would have low levels of AprA in the center of the colony, we observed that in images at lower magnification, the anti-Ras staining was detectable throughout the colony in colonies with 0.5 and 1×10^5 cells (Supplemental Figure 5). Colonies with 2×10^5 cells showed a ring, albeit one that extended farther toward the center of the colony than the ring seen with 4×10^5 cell colonies (Supplemental Figure 5). In agreement with the calculations, 8×10^5 cell colonies showed lower antigen detection by the anti-Ras antibody (Supplemental Figure 5). These data suggest that the inhibition of Ras activation at the cell cortex at the higher side of an AprA gradient is similar in cells at the margin of a colony to that in cells in a gradient chamber and that the effects of high levels of AprA may cause cells at the center of a colony to have different properties compared with cells at the edge of a colony.

GrlH, Gβ, Gα8, PakD, RasG, Erk1, and PKB are necessary for AprA to inhibit Ras activation

We previously identified mutants that have defective chemorepulsion from AprA (Bakthavatsalam *et al.*, 2009; Tang *et al.*, 2018; Rijal *et al.*, 2019), and in Figure 2C we observed that cells lacking GrlH do

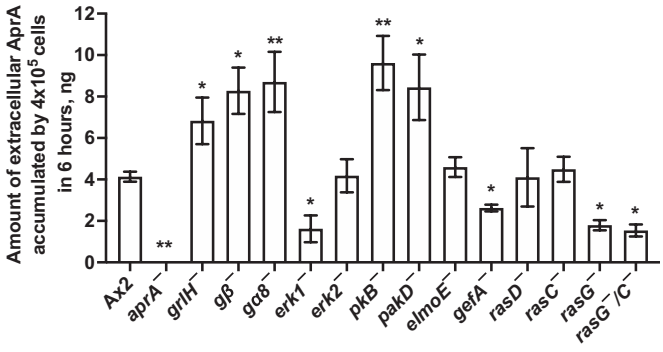

FIGURE 6: Extracellular accumulation of AprA. Spots of 4×10^5 cells of the indicated strains were placed in wells and allowed to adhere, and HL5 was gently added to the well. After 6 h, Western blots of the medium in the well were stained for AprA, using known quantities of rAprA as calibration standards. Values are mean ± SEM of four independent experiments. *$p < 0.05$, **$p < 0.01$ compared with Ax2 (unpaired *t* tests, Welch's correction).

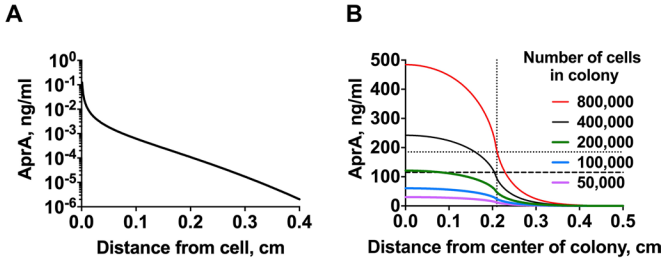

FIGURE 7: Predicted concentrations of AprA from diffusion calculations. (A) Theoretical concentration of AprA at the indicated distances from a single Ax2 cell on a solid surface continuously secreting AprA for 6 h. (B) Theoretical concentration of AprA close to the surface at different distances from the center of a colony of Ax2 cells on a surface after 6 h, with the indicated initial number of cells in the colony. The colony sizes match the colonies in Supplemental Figure 5. The vertical dotted line indicates the position of the edge of the colony at 6 h, the horizontal dotted line indicates 185 ng/ml AprA, and the horizontal dashed line indicates 115 ng/ml AprA.

not significantly decrease Ras cortical activation in response to AprA. To determine whether other proteins involved in chemorepulsion are needed for AprA to inhibit Ras activation, mutants were transformed with a Raf1-RBD-GFP construct and were then exposed to 300 ng/ml rAprA for 30 min and imaged. The localization of Raf1-RBD-GFP was examined in live cells. In addition to cells lacking GrlH, the loss of Gβ, Gα8, PakD, RasG, Erk1, and PKB blocked the ability of rAprA to decrease cortical Ras activation (Figure 9 and Supplemental Figure 6), suggesting that these proteins are necessary for, or are part of, the pathway from the AprA receptor to the Ras cortical activation inhibition. Although cells lacking Erk2 showed defective chemorepulsion from rAprA (Supplemental Figure 7), cells lacking Erk2 showed normal AprA-induced Ras deactivation from the cortical region (Figure 9 and Supplemental Figure 6). Cells lacking AprA, RasD, RasC, GefA, and ElmoE showed both the ability to chemorepel from a source of rAprA (Rijal *et al.*, 2019, and Supplemental Figure 7) and rAprA-induced Ras deactivation at the cortex (Figure 9 and Supplemental Figure 6).

To identify which proteins required for chemorepulsion are needed to affect Ras cortical activation in cells in a rAprA gradient, mutant cells were assessed for Raf1-RBD-GFP distribution as in Figure 1. As shown in Figure 10, in a rAprA gradient and compared with Ax2, there was no redistribution of Raf1-RBD-GFP intensity at the front and sides of the cell compared with the back (the region of the cell toward the source of rAprA) in cells lacking GrlH, Gβ, Gα8, PakD, RasG, Erk1, and PKB, suggesting that these proteins are necessary for, or are part of, the pathway from the AprA receptor to inhibit Ras cortical activation at the region of the cell closest to the AprA gradient (Figure 10 and Supplemental Figure 8). Cells lacking RasD and RasC showed an increase in Raf1-RBD-GFP intensity at the

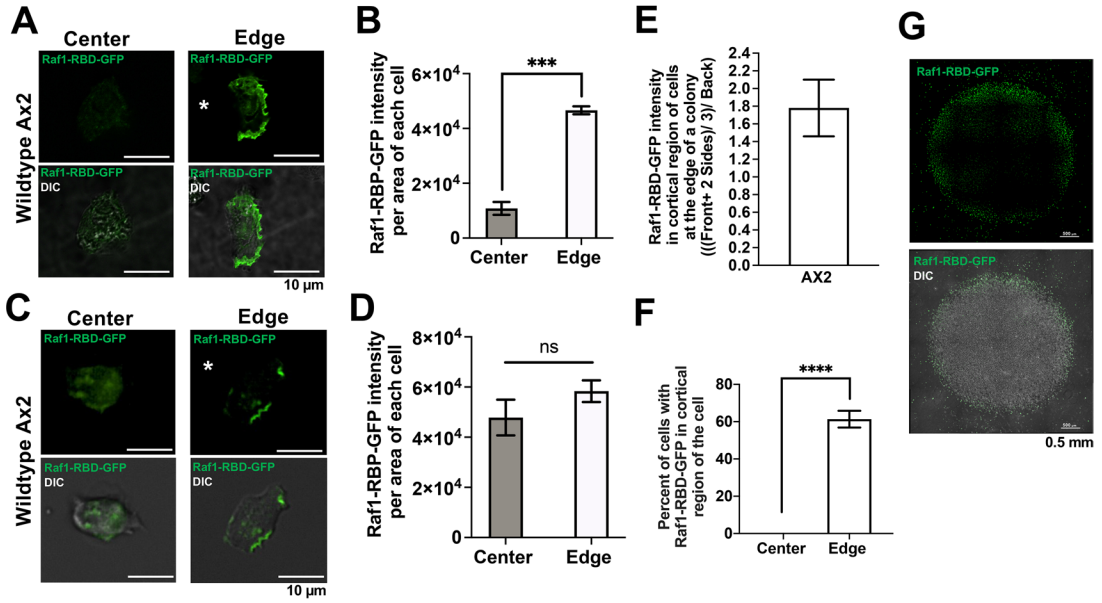

FIGURE 8: Extracellular accumulation of AprA inhibits Ras activation in cells at the center of a colony and redistributes Ras activation in cells at the edge of a colony. (A, C) Colonies of 4×10^5 Ax2 cells expressing Raf1-RBD-GFP (green) were incubated in HL5 for 6 h. The cells were then fixed (A) or imaged live (C). Cells at the center (left) and edge of the colony (right) were imaged. * indicates direction toward the center of the colony for cells at the edge. Bars are 10 µm. Images are representative of three independent experiments. (B) Graph shows the Raf1-RBD-GFP intensity per area (arbitrary units) in each cell located in the center and edge of the colony of fixed cells in A. (D) Graph shows the Raf1-RBD-GFP intensity per area (arbitrary units) in each cell located in the center and edge of the colony of live cell images (C). (E) Fixed cells at the edge of the colony were imaged and scored for the difference in Raf1-RBD-GFP intensity at the front and sides of the cell and at the back of the cell. Graph shows the ratio of ([Raf1-RBD-GFP intensity at the front and sides of the cells combined]/3) to (Raf1-RBD-GFP intensity at the back of the cell). (F) Graph shows the percent of cells with Ras cortical activation in fixed cells at the center and edge of the colony. Values are mean ± SEM of the averages from four independent experiments, with at least 90 randomly chosen cells examined for each point in each experiment. (G) Stitched images of a colony. Bars are 0.5 mm. Images are representative of three independent experiments. For B and F, ***$p < 0.001$, ****$p < 0.0001$ (unpaired *t* tests, Welch's correction).

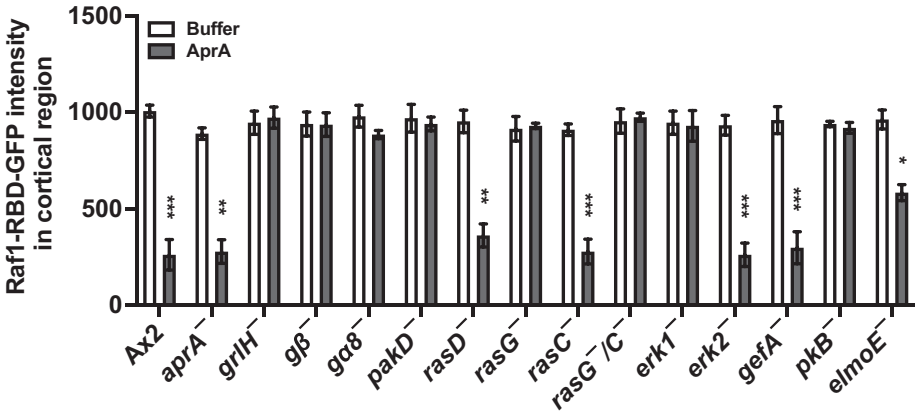

FIGURE 9: AprA does not inhibit Ras cortical activation in some mutants. Wild-type Ax2 and mutant cells were incubated in the presence or absence (buffer) of a uniform concentration of 300 ng/ml of rAprA for 60 min. Live cells expressing Raf1-RBD-GFP were imaged. Graph shows Raf1-RBD-GFP expression intensity in arbitrary units at the cortical region of the cells. Values are mean ± SEM of the averages from three independent experiments, with at least 36 randomly chosen cells examined for each condition in each experiment. *$p < 0.05$, **$p < 0.01$, ***$p < 0.001$ comparing buffer to AprA for each strain (two-way ANOVA, Holm-Šídák's test).

front and sides of the cells compared with the back of the cell, similar to Ax2 cells (Figure 10). Although required for chemorepulsion, cells lacking Erk2 showed Raf1-RBD-GFP intensity at the front and sides of the cells compared with the back of the cell similar to that of Ax2 cells (Figure 10). This suggests that Erk2 is necessary for, or is part of, pathways parallel to or downstream from Ras. Cells lacking GefA showed an intermediate phenotype in rAprA gradients; there was an enhancement of Raf1-RBD-GFP at the edge of the cell away from the source or rAprA, but there was still Raf1-RBD-GFP in other parts of the cell. For unknown reasons, in cells incubated in a uniform concentration of rAprA, Raf1-RBD-GFP seems to localize on cytosolic vesicles and pseudopods, whereas in cells incubated in a gradient of rAprA, Raf1-RBD-GFP seems to localize mostly in pseudopods (Supplemental Figures 6 and 8). To test whether these mutants accumulate extracellular AprA to generate an endogenous AprA gradient, the extracellular AprA accumulation by colonies of cells was measured. Except for *aprA*⁻ cells, all the mutants examined accumulated extracellular AprA (Figure 6). Compared to wild-type Ax2, cells lacking PakD and Erk1 showed an increase in the percent of cells at the edge of the colony with cortical active Ras (Supplemental Figure 9), suggesting that these proteins inhibit Ras activation at the cortex. Conversely, cells lacking GrlH, Gβ, Gα8, RasG, PKB, and ElmoE had a decreased percentage of cells at the edge of the colony with cortical Ras activation (Supplemental Figure 9), suggesting that these proteins potentiate Ras activation at the cortex.

DISCUSSION

In a cAMP gradient, Ras activation occurs at the region of the cell toward the source of cAMP (Sasaki *et al.*, 2004; Zhang *et al.*, 2008; Kortholt *et al.*, 2013). Complementary to previous observations of Ras activation in starved *Dictyostelium* cells exposed to pulses of cAMP every 6 min for 5 h (Sasaki *et al.*, 2004), we observed that cells

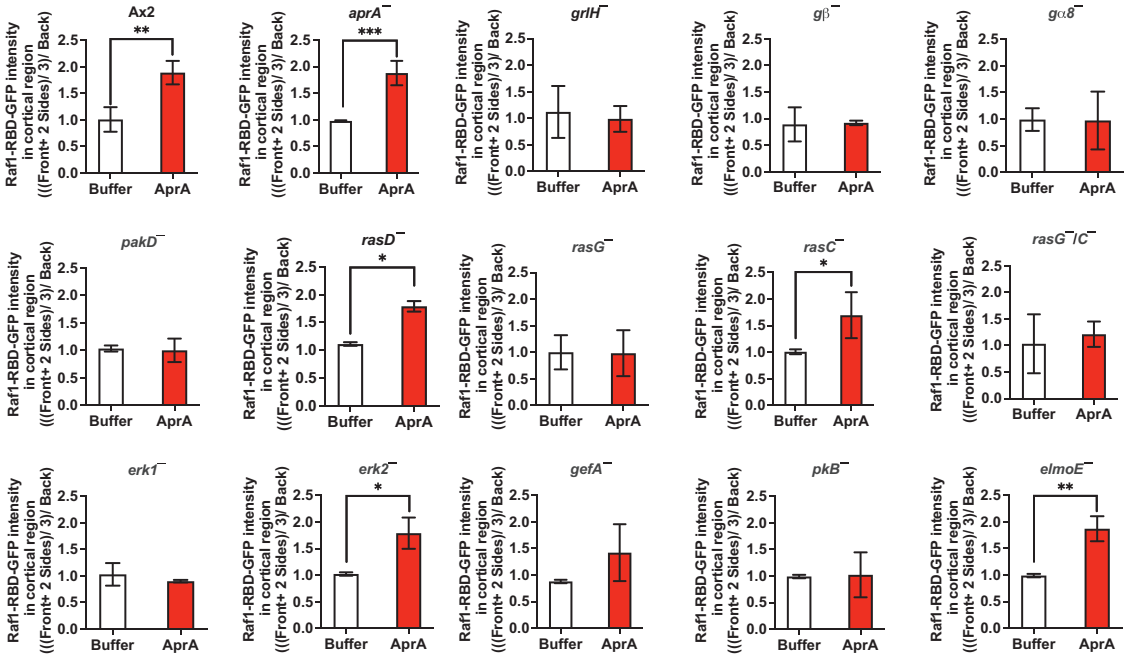

FIGURE 10: Ras cortical activation in cells in a rAprA gradient. Cells of the indicated genotypes expressing Raf1-RBD-GFP were exposed to a buffer or rAprA gradient. Images of live cells were taken. Graph shows the ratio of ([Raf1-RBD-GFP intensity at the front and sides of the cells combined]/3) to (Raf1-RBD-GFP intensity at the back of the cell). Values are mean ± SEM of the averages from four independent experiments, with at least 90 randomly chosen cells examined for each point in each experiment. *$p < 0.05$, **$p < 0.01$, ***$p < 0.001$ (unpaired *t* tests, Welch's correction).

in a nutrient-rich medium exposed to a continuous AprA gradient had Ras activation inhibited at the region of the cell toward the source of AprA. Similar to our observations, previous work has shown other examples of Ras inhibition to induce chemorepulsion. In human aortic endothelial cells, stimulation of EphB receptors by the growth cone chemorepellent ephrin-B1 increases local GAP levels to inhibit Ras activation (Lu *et al.*, 2001; Tong *et al.*, 2003; Noren and Pasquale, 2004; Schubbert *et al.*, 2007; Kao *et al.*, 2012; Lisabeth *et al.*, 2013). Combined with the work in this report, this then suggests that eukaryotes from *Dictyostelium* to humans have mechanisms where an extracellular signal can inhibit Ras activation.

Ras potentiates actin filament formation and pseudopod extension (Van Haastert *et al.*, 2017). Although the pathways of chemoattraction and chemorepulsion have many differences (Rijal *et al.*, 2019), for both cAMP and AprA, the redistribution of Ras activation thus appears to promote actin filament formation and pseudopod extension to allow the cell to have a biased movement. We previously found that in an AprA gradient, the percent of cells with pseudopods at the front of the cells increased and the percent of cells with pseudopod in the back decreased compared with those in control (Rijal *et al.*, 2019). Although pseudopod formation shifted from the rear to the front of the cells in an AprA gradient, pseudopod formation frequency did not significantly change compared with that in cells in a buffer gradient (Rijal *et al.*, 2019). Overall, Ras activation redistribution and the shift in pseudopod formation cause the cells to move in a biased direction away from the AprA. AprA concentrations above 115 ng/ml inhibited Ras activation.

We previously found that a uniform concentration of 2 µg/ml of AprA did not significantly affect cell speed (Phillips and Gomer, 2012), whereas here we observed that 300 ng/ml AprA decreased cell speed and increased cell roundness. An explanation for this difference could be that a saturation of AprA receptors due to the high concentration of AprA (2 µg/ml) (Phillips and Gomer, 2012) caused the cells to be insensitive to AprA.

In low-density vegetative cells (which will have low levels of accumulated extracellular AprA), we observed that Raf1-RBD-GFP tends to localize at the plasma membrane or on vesicles. One possibility is that these vesicles are pieces of the plasma membrane that have been internalized during macropinocytosis (Bloomfield *et al.*, 2015; Buckley *et al.*, 2020) and that there is some activation of Ras on the plasma membrane, as well as the internalized plasma membrane forming the macropinosomes. The Raf1-RBD-GFP would then bind the active Ras on the plasma membrane and in vesicles. The global addition of AprA caused the Raf1-RBD-GFP to show a diffuse distribution in cells. A possible explanation for this is that some of the AprA became engulfed in macropinosomes, the extracellular AprA inhibited Ras activation on the plasma membrane, and the engulfed AprA inhibited Ras on the macropinosomes. The absence of active Ras would then cause the Raf1-RBD-GFP to not have anything to bind to, resulting in a cytosolic distribution.

RasC and RasG are required for AprA-induced chemorepulsion (Rijal *et al.*, 2019). Although Raf1-RBD-GFP binds to active Ras, it does not bind to RasC (Kae *et al.*, 2004). In *Dictyostelium*, there are 14 characterized Ras proteins (Williams *et al.*, 2019). In cells lacking RasG and both RasG/C, Raf1-RBD-GFP appears to bind to active Ras both at the membrane and on cytosolic vesicles. Therefore, Raf1-RBD-GFP may be binding to other Ras proteins. This could indicate that RasG might have a role in regulating the binding of Raf1-RBD-GFP to other Ras proteins, excluding RasC, to inhibit signaling propagation after Ras activation.

GrlH, Gβ, Gα8, PakD, Erk1, RasG, and PKB are required for AprA-induced chemorepulsion (Phillips and Gomer, 2014; Rijal *et al.*, 2019) and for the ability of a uniform concentration or a gradient of rAprA to inhibit or redistribute Ras cortical activation. These proteins thus either are in the pathway between the AprA receptor GrlH and the inhibition of Ras activation or are necessary for the pathway. In both human neutrophils and *Dictyostelium*, several proteins such as Rho GTPases play a role in negatively regulating Ras activation (Sahai *et al.*, 2001; Wang *et al.*, 2013) and thus may be additional components of the GrlH to Ras pathway. Erk2 is required for chemorepulsion but is not required for AprA to inhibit Ras activation and, therefore, is an example of a protein that is in a pathway downstream of, or parallel to, the GrlH to Ras pathway.

In response to a source of cAMP, G proteins locally activate Ras proteins at the leading edge of the cell (Liu *et al.*, 2018). In human leukocytes, G proteins activate downstream proteins such as phospholipase C and receptor tyrosine kinases that recruit SHC/growth factor receptor–bound protein 2 (GRB2) to activate Ras proteins (Artemenko *et al.*, 2014). PAKs are regulated by both Rho and Ras proteins and play a major role in actin cytoskeleton organization to promote cell chemotaxis in human neutrophils and growth axonal cone guidance in developing *Drosophila* neurons (Itakura *et al.*, 2013). In Rat-1 fibroblasts, PAKs indirectly increase levels of phosphorylated Erk1, leading to the indirect negative regulation of Ras activation (Frost *et al.*, 1997; Lu *et al.*, 1997; Tang *et al.*, 1999). In human neutrophils, Erk1 plays a critical role during chemoattraction toward FMLP (Waki *et al.*, 2003; Zhang *et al.*, 2016). Erk1 can regulate Ras activation by initiating a negative feedback loop that promotes the inactivation of Ras proteins by phosphorylating the Grb2/Son of Sevenless (SOS) complex that activates Ras (Eblen, 2018). The pathway between the GrlH receptor and localized inhibition of Ras cortical activation thus appears to use components known to regulate Ras.

In an AprA gradient, PakD is required for chemorepulsion and localizes at the region of the cell closest to the source of AprA (Phillips and Gomer, 2014; Rijal *et al.*, 2019), the same region of the cell where AprA inhibits Ras cortical activation. This suggests that PakD localization may inhibit Ras activation. PKB is a serine/threonine protein kinase that contains a plekstrin homology domain allowing it to bind to PIP3 at the plasma membrane (Khwaja *et al.*, 1997; Osaki *et al.*, 2004). Once bound to PIP3 at the membrane, PKB is phosphorylated by phosphoinositide-dependent kinase 1, activating downstream proteins to regulate chemotaxis (Sarbassov *et al.*, 2005). In a cAMP gradient, PKB is involved in phosphorylating a Ras signaling complex that negatively regulates RasC during chemoattraction (Charest *et al.*, 2010). PKB may therefore play a similar role in the AprA chemorepulsion pathway.

In *Dictyostelium* and neutrophils, Elmo forms a complex with Dock and acts as a guanine nucleotide exchange factor (GEF) to mediate GTP loading of Rho GTPases to promote fast cytoskeletal rearrangement and cell migration (Brugnera *et al.*, 2002; Erwig and Henson, 2008; Yan *et al.*, 2012; Wang *et al.*, 2016; Arandjelovic *et al.*, 2019; Xu and Jin, 2019). In *Dictyostelium,* Elmo/Dock interacts with Gβγ, which in turn activates RacB or Rac1 to promote actin filament formation and pseudopod extension in a cAMP gradient (Laurin and Côté, 2014; Wang *et al.*, 2016; Xu and Jin, 2019). ElmoE is not required for AprA-induced chemorepulsion (Rijal *et al.*, 2019) and is not required for the ability of a uniform concentration of rAprA to inhibit Ras cortical activation. Although ElmoE is required for short-term repulsive behavior in a rAprA gradient to alter Ras cortical activation for 1 h, it is not required for cells to move away from AprA after 1 h. This suggests that ElmoE is part of a fast mechanism that senses a gradient of AprA and is not required for the long-term repulsion of cells at the edge of a colony.

In addition to mediating AprA inhibition of Ras cortical activation, GrlH, Gβ, Gα8, PKB, and PakD appear to inhibit the extracellular accumulation of AprA (Figure 6). Erk1 and RasG also mediate AprA inhibition of Ras cortical activation, and these proteins, along with GefA, appear to potentiate extracellular accumulation of AprA (Figure 6). Because GrlH and the associated G proteins are the first step in sensing AprA, these results suggest that AprA, possibly to prevent a global shutdown of Ras activation in cells at the edge of a large or dense colony, uses a negative feedback loop to modestly inhibit its own extracellular accumulation, either by decreasing AprA production and/or secretion or by increasing AprA degradation. Erk1, RasG, and GefA thus appear to inhibit components in this feedback loop.

Ras proteins play a key role in both cell migration and proliferation (Bar-Sagi and Hall, 2000; Coleman *et al.*, 2004; Crowe, 2004; Sasaki and Firtel, 2009; Kortholt *et al.*, 2013). Mutations that cause inappropriate activation of Ras are associated with 27–30% of human cancers (Schubbert *et al.*, 2007; Hobbs *et al.*, 2016). There are many commonalities between components of chemoattraction pathways and the AprA chemorepulsion pathway with proteins that when mutated can lead to cancer (Fernández-Medarde and Santos, 2011; Gurung and Bhattacharjee, 2015). In addition to inducing chemorepulsion, AprA decreases *Dictyostelium* cell proliferation (Choe *et al.*, 2009). An intriguing possibility is that both effects of AprA are caused by AprA inhibition of Ras activation.

MATERIALS AND METHODS

Request a protocol through *Bio-protocol*.

Cell strains and culture

Dictyostelium discoideum strains were purchased from the *Dictyostelium* stock center (Fey *et al.*, 2013). The strains included Ax2, *grlH*$^-$ (DBS0350226) (Tang *et al.*, 2018), *gα8*$^-$ (DBS0236107) (Wu *et al.*, 1994), *gβ*$^-$ (DBS0236531) (Lilly *et al.*, 1993; Wu *et al.*, 1995; Peracino *et al.*, 1998), *aprA*$^-$ (DBS0235509) (Brock and Gomer, 2005), *pakD*$^-$ (DBS0350281) (Garcia *et al.*, 2014), *rasD*$^-$ (DBS0236860) (Wilkins *et al.*, 2000), *rasC*$^-$ (DBS0236853) (Lim *et al.*, 2001), *rasG*$^-$ (DBS0236862) (Bolourani *et al.*, 2006), *rasC*$^-$/*rasG*$^-$ (DBS0236858) (Bolourani *et al.*, 2006), *gefA*$^-$ (DBS0236896) (Insall *et al.*, 1996), *elmoE*$^-$ (DBS0350065) (Yan *et al.*, 2012), *erk1*$^-$ (DBS0350622) (Nguyen *et al.*, 2010), *erk2*$^-$ (DBS0350606) (Nguyen *et al.*, 2010), and *pkbA*$^-$ (DBS0349876) (Tang *et al.*, 2011). Cells were transformed with a pDm115Raf1-RBD construct (Kortholt and Van Haastert, 2008) by electroporation as previously described (Kuspa and Loomis, 1992; Rijal *et al.*, 2019). Cells were cultured as previously described with G418 or blasticidin as appropriate for transformants in HL5 medium (Formedium, Hunstanton, England) (Brock and Gomer, 1999; Rijal *et al.*, 2019).

rAprA and chemorepulsion assays

Recombinant AprA (rAprA) was expressed and purified as previously described (Bakthavatsalam *et al.*, 2008) and concentrated using a #431488 10 kDa cutoff Spin-X UF 20 centrifugal concentrator (Corning, Corning, NY). The rAprA was stored at 4°C in aliquots of ~200 ng/μl in 20 mM sodium phosphate, pH 7.4. Chemorepulsion assays using an Insall chamber were performed as previously described (Bakthavatsalam *et al.*, 2008; Rijal *et al.*, 2019). For chemorepulsion assays in eight-well chamber slides, cells were grown to 1×10^6 cells/ml in HL5 in shaking culture and collected by centrifugation at $500 \times g$ for 3 min. Cells were resuspended in HL5 and washed twice more by centrifugation and resuspension. The cells were then resuspended in HL5 to 1.0×10^5 cells/ml, and 300 μl was placed in a chamber of a #354118 eight-chamber tissue culture–treated glass slide (Corning) and allowed to adhere for 30 min at room temperature. From a 250–300 ng/μl rAprA stock in 20 mM $NaPO_4$, pH 7.4, ~0.5–0.8 μl was gently added to the corner of the well as previously described to make a rAprA gradient (Rijal *et al.*, 2019). Control wells had an equal volume of 20 mM $NaPO_4$, pH 7.4, added to the corner of the well. Cells were imaged after 20 min. For videomicroscopy, a similar experiment was done with the exception that the cells were in a 1:1 mixture of HL5 and SIH (Formedium), and cells in the center of the well were imaged every 15 s for 1 h at a low exposure level (5 ms of excitation light in the GFP channel every 15 s) to minimize photodamage using a Ti2 Eclipse microscope (Nikon, Melville, NY) with 10× and a PCO Tech 5.5 m cooled sCMOS microscope camera (PCO-Tech, Wilmington, DE). Each batch of rAprA was tested for chemorepulsion activity on wild-type cells before further experiments were performed. For each individual experiment, at least 40 cells were tracked.

Cell speed and roundness assays

The effect of rAprA on cells was done as described in Phillips and Gomer (2012) with the exception that cells were exposed to 300 ng/ml rAprA. Cell roundness and motility speed were measured as described in Wang *et al.* (2013) with the exception that for each individual experiment, at least 40 cells were analyzed.

Methylene blue dye diffusion assay

Methylene blue dye was used to assess gradient formation in the well of an eight-well slide. A 10× stock solution was made by adding 0.125 g of methylene blue (Sigma, St. Louis, MO) to 50 ml of distilled water. This was diluted 1:9 in HL5 and clarified by centrifugation at $500 \times g$ for 1 min. Diluted dye (2 μl) was then added to the corner of a well in a #354118 eight-chamber slide containing 200 μl of HL5. The well was then imaged at different times on a Ti2 Eclipse microscope with a 10× objective. FIJI ImageJ software (Schindelin *et al.*, 2012) was used to analyze and quantify the staining. Diffusion from a single added point was calculated as previously described (Yuen and Gomer, 1994).

Raf1-RBD localization in cells exposed to rAprA

For live cell imaging of cells in a rAprA gradient, cells were resuspended to 1×10^5 cells/ml and exposed to a gradient in the well of an eight-well slide for 30 min as described above. Differential interference contrast (DIC) and fluorescence images of live cells were taken with a 20× objective on a Nikon Ti2 Eclipse microscope. For live cell imaging of cells in a uniform concentration of rAprA, the cells were prepared as above. rAprA in 20 mM $NaPO_4$, pH 7.4, was added to a final concentration of 300 ng/ml, and this was mixed gently and then allowed to incubate for 30 min. Controls were treated similarly, adding an equal concentration of 20 mM $NaPO_4$, pH 7.4. For some experiments, the medium was gently removed after 1 h and 300 μl of fresh HL5 was added to each well. Images were taken with a 40× objective on a Nikon Ti2 Eclipse microscope. FIJI ImageJ software (Schindelin *et al.*, 2012) was used to analyze and quantify fluorescence. Quantification was done as previously described (Mouneimne *et al.*, 2006) with the exception that the ratio was ([integrated Raf1-RBD-GFP intensity in the cortical region at the front and sides of the cell]/3) divided by (integrated Raf1-RBD-GFP intensity in the cortical region at the back of the cell).

Raf1-RBD localization in 6-h-starved cells exposed to cAMP

For live cell imaging of cells expressing Raf1-RBD-GFP in a cAMP gradient, cells were grown and collected as described above and then resuspended in PBM (20 mM KH_2PO_4, 0.01 mM $CaCl_2$, 1 mM

$MgCl_2$, pH adjusted to 6.1 using KOH) to 1×10^6 cells/ ml and allowed to starve for 6 h. The cells were then collected as described above and washed twice with PBM and resuspended in PBM to 1.0×10^5 cells/ml. Three hundred microliters was placed in an eight-well slide and allowed to adhere for 30 min. cAMP (0.3 µl) (R8196; Denville Scientific, Metuchen, NJ), from a 1 mM stock in sterile water, was gently added to the corner of the well. DIC and fluorescence images of live cells were taken with a 20× objective on a Nikon Ti2 Eclipse microscope.

Ras protein levels

To measure Ras protein levels in cells after treatment with different concentrations of rAprA, the cells were grown in HL5 in shaking culture and collected as described above. Different concentrations of rAprA or equal volumes of sodium phosphate buffer were gently added to each well and left for 6 h. The medium was gently removed, and 200 µl of 1× SDS sample buffer with 1× #1861281 protease and phosphatase cocktail inhibitor (Thermo Scientific, Waltham, MA) was added to each well. The lysates were then heated to 95°C for 5 min. Samples were electrophoresed and blotted as previously described (Bakthavatsalam *et al.*, 2008) with the exceptions that the blots were blocked in 5% nonfat skim milk (Difco, Franklin Lakes, NJ) in phosphate-buffered saline (PBS) with 0.1% Tween 20 (PBST) for 1 h, stained as previously described (Rijal *et al.*, 2019) with 1:250 #AESA02 anti-Ras antibody (Cytoskeleton, Denver, CO), and the secondary antibody was 1:2500 #715-036-150 peroxidase-conjugated donkey anti-mouse immunoglobulin G (Jackson ImmunoResearch). Staining was detected with a SuperSignal West Pico PLUS Chemiluminescent Substrate for 10 min (Cat. #34087, Thermo). Images of the membrane were taken using a BioRad ChemiDoc XRS system and quantified using Image Lab software (BioRad).

Ras pull-down assays

Ras activation was measured using pull-down assay kits (BK008-S; Cytoskeleton) following the manufacturer's protocol with the exception that 4×10^6 cells/ml were incubated in HL5 with 1 ml/well in 24-well plates. After allowing the cells to adhere for 30 min, they were treated with 300 ng/ml rAprA, adding the appropriate volume of a typically 200 µg/ml stock of rAprA in 20 mM sodium phosphate, pH 7.4, or the same volume of sodium phosphate buffer for 0, 5, 10, 20, 30, 60 min. The supernatant was removed and replaced with 200 µl of RIPA buffer (Cat. #UG286842; Thermo) to lyse the cells. Image Lab software (BioRad) was used for quantitation of the immunoblot. Band intensities were normalized to the total lane intensity of Coomassie-stained gels of the corresponding cell sample, and this was then normalized to the band intensity of total Ras protein in Western blots of the cell sample.

Cell colony assays

Cells growing in HL5 were collected at log phase and washed as described above, resuspended to 4×10^5 cells/ml in HL5, and cells (4 µl) were spotted into the center of a chamber in an eight-chamber slide. After 30 min in a humid chamber, 200 µl of HL5 was slowly added to the chamber from the corner. The slides were incubated for 6 h in a humid chamber, then 100 µl of the medium was gently removed, and 200 µl of 4% paraformaldehyde in phosphate-buffered saline (PBS) was added to each well. The cells were fixed and stained as described in Rijal *et al.* (2019) using a 1:500 dilution of a primary antibody that stains a Ras antigen (#AESA02; Cytoskeleton) followed by a 1:1000 dilution of secondary antibody (#715-546-150 Alexa Fluor 488 donkey anti-mouse; Jackson ImmunoResearch, West Grove, PA). For live images of the colonies, a similar experiment was done with cells expressing Raf1-RBD-GFP. The colonies were then imaged using a DM6B confocal microscope (Leica Microsystems, Wetzlar, Germany) with a Plan Apo Lambda 10× dry objective. The images were stitched using LAS X software (Leica Microsystems). Higher-magnification images of the cells at the edge of a colony were taken on a Nikon Ti2 Eclipse microscope (Nikon) with a 40× objective. FIJI ImageJ software (Schindelin *et al.* 2012) was used to analyze and quantify the staining. For each individual experiment, Ras antigen and Raf1-RBD-GFP localization were assessed in at least 40 randomly chosen cells at the edge of a colony.

AprA concentration measurements of cell supernatants

Colonies of cells were made as described above. After 6 h, the medium was collected and clarified by centrifugation at $500 \times g$ for 3 min. The supernatant was then transferred to a Spin-XR UF 500 30k MWCO PES concentrator (Corning) and centrifuged at $12{,}000 \times g$ for 5 min. The retentate in the concentrator was adjusted to 200 µl using PBS and was mixed with 1× SDS sample buffer and heated to 95°C for 5 min. Western blots of samples and known quantities of rAprA were stained for Ras as described above.

Statistics

Statistical analyses were done using Prism version 8.4.1 (GraphPad, San Diego, CA) for *t* tests and one-way or two-way analysis of variance (ANOVA) with appropriate posttests. Significance was defined as $p < 0.05$.

ACKNOWLEDGMENTS

We thank Chance Hatfield for performing blinded experiments to replicate results. The use of the Microscopy and Imaging Center facility at Texas A&M University is acknowledged. We thank Ramesh Rijal, Darrell Pilling and Kristen Consalvo for helping to improve the clarity of the manuscript. This work was supported by National Institutes of Health Grants R01 GM118355 and R35 GM139486.

REFERENCES

Adhikari N, Kuburich NA, Hadwiger JA (2020). Mitogen-activated protein kinase regulation of the phosphodiesterase RegA in early Dictyostelium development. Microbiology (Reading) 166, 129–140.

Ananthakrishnan R, Ehrlicher A (2007). The forces behind cell movement. Intl J Biol Sci 3, 303–317.

Arandjelovic S, Perry JSA, Lucas CD, Penberthy KK, Kim T-H, Zhou M, Rosen DA, Chuang T-Y, Bettina AM, Shankman LS, *et al.* (2019). A noncanonical role for the engulfment gene ELMO1 in neutrophils that promotes inflammatory arthritis. Nat Immunol 20, 141–151.

Artemenko Y, Lampert TJ, Devreotes PN (2014). Moving towards a paradigm: common mechanisms of chemotactic signaling in Dictyostelium and mammalian leukocytes. Cell Mol Life Sci 71, 3711–3747.

Bagorda A, Parent CA (2008). Eukaryotic chemotaxis at a glance. J Cell Sci 121, 2621.

Bakthavatsalam D, Brock DA, Nikravan NN, Houston KD, Hatton RD, Gomer RH (2008). The secreted Dictyostelium protein CfaD is a chalone. J Cell Sci 121, 2473–2480.

Bakthavatsalam D, Choe JM, Hanson NE, Gomer RH (2009). A *Dictyostelium* chalone uses G proteins to regulate proliferation. BMC Biol 7, 44.

Bar-Sagi D, Hall A (2000). Ras and Rho GTPases: a family reunion. Cell 103, 227–238.

Bloomfield G, Traynor D, Sander SP, Veltman DM, Pachebat JA, Kay RR (2015). Neurofibromin controls macropinocytosis and phagocytosis in Dictyostelium. eLife 4, e04940.

Bolourani P, Spiegelman GB, Weeks G (2006). Delineation of the roles played by RasG and RasC in cAMP-dependent signal transduction during the early development of Dictyostelium discoideum. Mol Biol Cell 17, 4543–4550.

Bosgraaf L, Van Haastert PJM (2009). Navigation of chemotactic cells by parallel signaling to pseudopod persistence and orientation. PLoS One 4, e6842.

Bourne HR, Sanders DA, McCormick F (1991). The GTPase superfamily: conserved structure and molecular mechanism. Nature 349, 117–127.
Bretschneider T, Othmer HG, Weijer CJ (2016). Progress and perspectives in signal transduction, actin dynamics, and movement at the cell and tissue level: lessons from Dictyostelium. Interface Focus 6, 20160047.
Brock DA, Gomer RH (1999). A cell-counting factor regulating structure size in Dictyostelium. Genes Dev 13, 1960–1969.
Brock DA, Gomer RH (2005). A secreted factor represses cell proliferation in Dictyostelium. Development 132, 4553–4562.
Brugnera E, Haney L, Grimsley C, Lu M, Walk SF, Tosello-Trampont AC, Macara IG, Madhani H, Fink GR, Ravichandran KS (2002). Unconventional Rac-GEF activity is mediated through the Dock180-ELMO complex. Nat Cell Biol 4, 574–582.
Buckley CM, Pots H, Gueho A, Vines JH, Munn CJ, Phillips BA, Gilsbach B, Traynor D, Nikolaev A, Soldati T, *et al*. (2020). Coordinated Ras and Rac activity shapes macropinocytic cups and enables phagocytosis of geometrically diverse bacteria. Curr Biol 30, 2912–2926.e5.
Cai H, Das S, Kamimura Y, Long Yu, Parent CA, Devreotes PN (2010). Ras-mediated activation of the TORC2-PKB pathway is critical for chemotaxis. J Cell Biol 190, 233–245.
Charest PG, Shen Z, Lakoduk A, Sasaki AT, Briggs SP, Firtel RA (2010). A Ras signaling complex controls the RasC-TORC2 pathway and directed cell migration. Dev Cell 18, 737–749.
Chen L, Iijima M, Tang M, Landree MA, Huang YE, Xiong Y, Iglesias PA, Devreotes PN (2007). PLA2 and PI3K/PTEN pathways act in parallel to mediate chemotaxis. Dev Cell 12, 603–614.
Cheng Y, Felix B, Othmer HG (2020). The roles of signaling in cytoskeletal changes, random movement, direction-sensing and polarization of eukaryotic cells. Cells 9, 1437.
Choe JM, Bakthavatsalam D, Phillips JE, Gomer RH (2009). Dictyostelium cells bind a secreted autocrine factor that represses cell proliferation. BMC Biochem 10, 4.
Coleman ML, Marshall CJ, Olson MF (2004). RAS and RHO GTPases in G1-phase cell-cycle regulation. Nat Rev Mol Cell Biol 5, 355–366.
Cooper RM, Wingreen NS, Cox EC (2012). An excitable cortex and memory model successfully predicts new pseudopod dynamics. PLoS One 7, e33528.
Crowe DL (2004). Overlapping functions of Ras and Rac GTPases in regulating cancer cell proliferation and invasion. Anticancer Res 24, 593–597.
De Palo G, Yi D, Endres RG (2017). A critical-like collective state leads to long-range cell communication in Dictyostelium discoideum aggregation. PLoS Biol 15, e1002602.
Devreotes PN, Zigmond SH (1988). Chemotaxis in eukaryotic cells: a focus on leukocytes and Dictyostelium. Annu Rev Cell Biol 4, 649–686.
Eblen ST (2018). Extracellular-regulated kinases: signaling from Ras to ERK substrates to control biological outcomes. Adv Cancer Res 138, 99–142.
Eidi Z (2017). Discrete modeling of amoeboid locomotion and chemotaxis in Dictyostelium discoideum by tracking pseudopodium growth direction. Sci Rep 7, 12675.
Erwig LP, Henson PM (2008). Clearance of apoptotic cells by phagocytes. Cell Death Differ 15, 243–250.
Fernández-Medarde A, Santos E (2011). Ras in cancer and developmental diseases. Genes Cancer 2, 344–358.
Fey P, Dodson RJ, Basu S, Chisholm RL (2013). One stop shop for everything Dictyostelium: dictyBase and the Dicty Stock Center in 2012. In: Dictyostelium discoideum Protocols, ed. L Eichinger and F Rivero, Totowa, NJ: Humana Press.
Frost JA, Steen H, Shapiro P, Lewis T, Ahn N, Shaw PE, Cobb MH (1997). Cross-cascade activation of ERKs and ternary complex factors by Rho family proteins. EMBO J 16, 6426–6438.
Garcia GL, Parent CA (2008). Signal relay during chemotaxis. J Microsc 231, 529–534.
Garcia M, Ray S, Brown I, Irom J, Brazill D (2014). PakD, a putative p21-activated protein kinase in Dictyostelium discoideum, regulates actin. Eukaryot Cell 13, 119–126.
Goldberg D, Borojevic R, Anderson M, Chen JJ, Gershon MD, Ratcliffe EM (2013). Slit/Robo-mediated chemorepulsion of vagal sensory axons in the fetal gut. Dev Dyn 242, 9–15.
Gomer RH (2019). The use of diffusion calculations and monte carlo simulations to understand the behavior of cells in dictyostelium communities. Comput Struct Biotechnol J 17, 684–688.
Gurung A, Bhattacharjee A (2015). Significance of Ras signaling in cancer and strategies for its control. Oral Hist Rev 11, 147.
Havlioglu N, Yuan L, Tang H, Wu JY (2002). Slit proteins, potential endogenous modulators of inflammation. J Neurovirol 8, 486–495.
Heid PJ, Geiger J, Wessels D, Voss E, Soll DR (2005). Computer-assisted analysis of filopod formation and the role of myosin II heavy chain phosphorylation in *Dictyostelium*. J Cell Sci 118, 2225–2237.
Herlihy SE, Brown ML, Pilling D, Weeks BR, Myers LK, Gomer RH (2015). Role of the neutrophil chemorepellent soluble dipeptidyl peptidase IV in decreasing inflammation in a murine model of arthritis. Arthritis Rheumatol 67, 2634–2638.
Herlihy SE, Pilling D, Maharjan AS, Gomer RH (2013). Dipeptidyl peptidase IV is a human and murine neutrophil chemorepellent. J Immunol 190, 6468–6477.
Herlihy SE, Tang Y, Phillips JE, Gomer RH (2017). Functional similarities between the dictyostelium protein AprA and the human protein dipeptidyl-peptidase IV. Protein Sci 26, 578–585.
Hobbs GA, Der CJ, Rossman KL (2016). RAS isoforms and mutations in cancer at a glance. J Cell Sci 129, 1287–1292.
Hu H (1999). Chemorepulsion of neuronal migration by Slit2 in the developing mammalian forebrain. Neuron 23, 703–711.
Insall RH, Borleis J, Devreotes PN (1996). The aimless RasGEF is required for processing of chemotactic signals through G-protein-coupled receptors in Dictyostelium. Curr Biol 6, 719–729.
Itakura A, Aslan JE, Kusanto BT, Phillips KG, Porter JE, Newton PK, Nan X, Insall RH, Chernoff J, McCarty OJT (2013). p21-activated kinase (PAK) regulates cytoskeletal reorganization and directional migration in human neutrophils. PLoS One 8, e73063.
Janetopoulos C, Firtel RA (2008). Directional sensing during chemotaxis. FEBS Lett 582, 2075–2085.
Kae H, Lim CJ, Spiegelman GB, Weeks G (2004). Chemoattractant-induced Ras activation during Dictyostelium aggregation. EMBO Rep 5, 602–606.
Kao TJ, Law C, Kania A (2012). Eph and ephrin signaling: lessons learned from spinal motor neurons. Semin Cell Dev Biol 23, 83–91.
Khwaja A, Rodriguez-Viciana P, Wennström S, Warne PH, Downward J (1997). Matrix adhesion and Ras transformation both activate a phosphoinositide 3-OH kinase and protein kinase B/Akt cellular survival pathway. EMBO J 16, 2783–2793.
Kim JY, Borleis JA, Devreotes PN (1998). Switching of chemoattractant receptors programs development and morphogenesis in Dictyostelium: receptor subtypes activate common responses at different agonist concentrations. Dev Biol 197, 117–128.
King JS, Insall RH (2009). Chemotaxis: finding the way forward with Dictyostelium. Trends Cell Biol 19, 523–530.
Kortholt A, Van Haastert PJM (2008). Highlighting the role of Ras and Rap during Dictyostelium chemotaxis. Cell Signal 20, 1415–1422.
Kortholt A, Kataria R, Keizer-Gunnink I, Van Egmond WN, Khanna A, Van Haastert PJ (2011). Dictyostelium chemotaxis: essential Ras activation and accessory signalling pathways for amplification. EMBO Rep 12, 1273–1279.
Kortholt A, Keizer-Gunnink I, Kataria R, Van Haastert PJM (2013). Ras activation and symmetry breaking during *Dictyostelium* chemotaxis. J Cell Sci 126, 4502.
Kuspa A, Loomis WF (1992). Tagging developmental genes in Dictyostelium by restriction enzyme-mediated integration of plasmid DNA. Proc Natl Acad Sci USA 89, 8803.
Kyriakis JM, App H, Zhang XF, Banerjee P, Brautigan DL, Rapp U, Avruch J (1992). Raf-1 activates MAP kinase-kinase. Nature 358, 417–421.
Lake D, Corrêa SA, Müller J (2016). Negative feedback regulation of the ERK1/2 MAPK pathway. Cell Mol Life Sci 73, 4397–4413.
Laurin M, Côté J-F (2014). Insights into the biological functions of Dock family guanine nucleotide exchange factors. Genes Dev 28, 533–547.
Li X, Edwards M, Swaney KF, Singh N, Bhattacharya S, Borleis J, Long Y, Iglesias PA, Chen J, Devreotes PN (2018). Mutually inhibitory Ras-PI(3,4)P(2) feedback loops mediate cell migration. Proc Natl Acad Sci USA 115, E9125–e34.
Lilly P, Wu L, Welker DL, Devreotes PN (1993). A G-protein beta-subunit is essential for Dictyostelium development. Genes Dev 7, 986–995.
Lim CJ, Spiegelman GB, Weeks G (2001). RasC is required for optimal activation of adenylyl cyclase and Akt/PKB during aggregation. EMBO J 20, 4490–4499.
Lisabeth EM, Falivelli G, Pasquale EB (2013). Eph receptor signaling and ephrins. Cold Spring Harb Perspect Biol 5, a009159.
Liu Y, Lacal J, Firtel RA, Kortholt A (2018). Connecting G protein signaling to chemoattractant-mediated cell polarity and cytoskeletal reorganization. Small GTPases 9, 360–364.
Lu Q, Sun EE, Klein RS, Flanagan JG (2001). Ephrin-B reverse signaling is mediated by a novel PDZ-RGS protein and selectively inhibits G protein-coupled chemoattraction. Cell 105, 69–79.

Lu W, Katz S, Gupta R, Mayer BJ (1997). Activation of Pak by membrane localization mediated by an SH3 domain from the adaptor protein Nck. Curr Biol 7, 85–94.
Ma H, Gamper M, Parent C, Firtel RA (1997). The Dictyostelium MAP kinase kinase DdMEK1 regulates chemotaxis and is essential for chemoattractant-mediated activation of guanylyl cyclase. EMBO J 16, 4317–4332.
Mouneimne G, DesMarais V, Sidani M, Scemes E, Wang W, Song X, Eddy R, Condeelis J (2006). Spatial and temporal control of cofilin activity is required for directional sensing during chemotaxis. Curr Biol 16, 2193–2205.
Nguyen-Ba-Charvet KT, Brose K, Marillat V, Kidd T, Goodman CS, Tessier-Lavigne M, Sotelo C, Chedotal A (1999). Slit2-mediated chemorepulsion and collapse of developing forebrain axons. Neuron 22, 463–473.
Nguyen HN, Raisley B, Hadwiger JA (2010). MAP kinases have different functions in Dictyostelium G protein-mediated signaling. Cell Signal 22, 836–847.
Nichols JME, Paschke P, Peak-Chew S, Williams TD, Tweedy L, Skehel M, Stephens E, Chubb JR, Kay RR (2019). The atypical MAP kinase ErkB transmits distinct chemotactic signals through a core signaling module. Dev Cell 48, 491–505.e9.
Noren NK, Pasquale EB (2004). Eph receptor–ephrin bidirectional signals that target Ras and Rho proteins. Cell Signal 16, 655–666.
Osaki M, Oshimura M, Ito H (2004). PI3K-Akt pathway: its functions and alterations in human cancer. Apoptosis 9, 667–676.
Pal DS, Li X, Banerjee T, Miao Y, Devreotes PN (2019). The excitable signal transduction networks: movers and shapers of eukaryotic cell migration. Int J Dev Biol 63, 407–416.
Peracino B, Borleis J, Jin T, Westphal M, Schwartz JM, Wu L, Bracco E, Gerisch G, Devreotes P, Bozzaro S (1998). G protein beta subunit-null mutants are impaired in phagocytosis and chemotaxis due to inappropriate regulation of the actin cytoskeleton. J Cell Biol 141, 1529–1537.
Petri B, Sanz MJ (2018). Neutrophil chemotaxis. Cell Tissue Res 371, 425–436.
Phillips JE, Gomer RH (2012). A secreted protein is an endogenous chemorepellant in Dictyostelium discoideum. Proc Natl Acad Sci USA 109, 10990–10995.
Phillips JE, Gomer RH (2014). The p21-activated kinase (PAK) family member PakD is required for chemorepulsion and proliferation inhibition by autocrine signals in Dictyostelium discoideum. PLoS One 9, e96633.
Pilling D, Chinea LE, Consalvo KM, Gomer RH (2019). Different isoforms of the neuronal guidance molecule Slit2 directly cause chemoattraction or chemorepulsion of human neutrophils. J Immunol 202, 239–248.
Postma M, Roelofs J, Goedhart J, Gadella TWJ, Visser AJWG, Van Haastert PJM (2003). Uniform cAMP stimulation of Dictyostelium cells induces localized patches of signal transduction and pseudopodia. Mol Biol Cell 14, 5019–5027.
Rappel W-J, Edelstein-Keshet L (2017). Mechanisms of cell polarization. Curr Opin Syst Biol 3, 43–53.
Rappel W-J, Loomis WF (2009). Eukaryotic chemotaxis. Wiley Interdiscip Rev Syst Biol Med 1, 141–149.
Ridley AJ (2001). Rho GTPases and cell migration. J Cell Sci 114, 2713–2722.
Rijal R, Consalvo KM, Lindsey CK, Gomer RH (2019). An endogenous chemorepellent directs cell movement by inhibiting pseudopods at one side of cells. Mol Biol Cell 30, 242–255.
Sahai E, Olson MF, Marshall CJ (2001). Cross-talk between Ras and Rho signalling pathways in transformation favours proliferation and increased motility. EMBO J 20, 755–766.
Saran S, Meima ME, Alvarez-Curto E, Weening KE, Rozen DE, Schaap P (2002). cAMP signaling in Dictyostelium. Complexity of cAMP synthesis, degradation and detection. J Muscle Res Cell Motil 23, 793–802.
Sarbassov DD, Guertin DA, Ali SM, Sabatini DM (2005). Phosphorylation and regulation of Akt/PKB by the rictor-mTOR complex. Science 307, 1098–1101.
Sasaki AT, Chun C, Takeda K, Firtel RA (2004). Localized Ras signaling at the leading edge regulates PI3K, cell polarity, and directional cell movement. J Cell Biol 167, 505–518.
Sasaki AT, Firtel RA (2009). Spatiotemporal regulation of Ras-GTPases during chemotaxis. In: Chemotaxis: Methods and Protocols, ed. T Jin and D Hereld, Totowa, NJ: Humana Press.
Schindelin J, Arganda-Carreras I, Frise E, Kaynig V, Longair M, Pietzsch T, Preibisch S, Rueden C, Saalfeld S, Schmid B, *et al*. (2012). Fiji: an open-source platform for biological-image analysis. Nat Methods 9, 676–682.
Schubbert S, Shannon K, Bollag G (2007). Hyperactive Ras in developmental disorders and cancer. Nat Rev Cancer 7, 295–308.
Schwartz MA, Horwitz AR (2006). Integrating adhesion, protrusion, and contraction during cell migration. Cell 125, 1223–1225.
Singer G, Araki T, Weijer CJ (2019). Oscillatory cAMP cell-cell signalling persists during multicellular Dictyostelium development. Commun Biol 2, 139.
Stepanovic V, Wessels D, Daniels K, Loomis WF, Soll DR (2005). Intracellular role of adenylyl cyclase in regulation of lateral pseudopod formation during Dictyostelium chemotaxis. Eukaryot Cell 4, 775–786.
Suire S, Condliffe AM, Ferguson GJ, Ellson CD, Guillou H, Davidson K, Welch H, Coadwell J, Turner M, Chilvers ER, *et al*. (2006). Gβγs and the Ras binding domain of p110γ are both important regulators of PI3Kγ signalling in neutrophils. Nat Cell Biol 8, 1303–1309.
Tang M, Iijima M, Kamimura Y, Chen L, Long Yu, Devreotes P (2011). Disruption of PKB signaling restores polarity to cells lacking tumor suppressor PTEN. Mol Biol Cell 22, 437–447.
Tang Y, Wu Y, Herlihy SE, Brito-Aleman FJ, Ting JH, Janetopoulos C, Gomer RH (2018). An autocrine proliferation repressor regulates Dictyostelium discoideum proliferation and chemorepulsion using the G protein-coupled receptor GrlH. mBio 9, e02443–17.
Tang Y, Yu J, Field J (1999). Signals from the Ras, Rac, and Rho GTPases converge on the Pak protein kinase in Rat-1 fibroblasts. Mol Cell Biol 19, 1881.
Thomas MA, Kleist AB, Volkman BF (2018). Decoding the chemotactic signal. J Leukoc Biol 104, 359–374.
Tong J, Elowe S, Nash P, Pawson T (2003). Manipulation of EphB2 regulatory motifs and SH2 binding sites switches MAPK signaling and biological activity. J Biol Chem 278, 6111–6119.
Uchida KSK, Yumura S (2004). Dynamics of novel feet of Dictyostelium cells during migration. J Cell Sci 117, 1443.
Van Haastert PJM (2010). Chemotaxis: insights from the extending pseudopod. J Cell Sci 123, 3031.
Van Haastert PJM, Keizer-Gunnink I, Kortholt A (2017). Coupled excitable Ras and F-actin activation mediates spontaneous pseudopod formation and directed cell movement. Mol Biol Cell 28, 922–934.
Veltman DM, Keizer-Gunnik I, Van Haastert PJM (2008). Four key signaling pathways mediating chemotaxis in Dictyostelium discoideum. The J Cell Biol 180, 747–753.
Waki K, Inanami O, Yamamori T, Kuwabara M (2003). Extracellular signal-regulated kinase 1/2 is involved in the activation of NADPH oxidase induced by FMLP receptor but not by complement receptor 3 in rat neutrophils. Free Radic Res 37, 665–671.
Wang Y, Senoo H, Sesaki H, Iijima M (2013). Rho GTPases orient directional sensing in chemotaxis. Proc Natl Acad Sci USA 110, E4723–E4732.
Wang Y, Xu X, Pan M, Jin T (2016). ELMO1 directly interacts with Gβγ subunit to transduce GPCR signaling to Rac1 activation in chemotaxis. J Cancer 7, 973–983.
Wennerberg K, Rossman KL, Der CJ (2005). The Ras superfamily at a glance. J Cell Sci 118, 843–846.
White MJV, Chinea LE, Pilling D, Gomer RH (2018). Protease activated-receptor 2 is necessary for neutrophil chemorepulsion induced by trypsin, tryptase, or dipeptidyl peptidase IV. J Leukoc Biol 103, 119–128.
Wilkins A, Khosla M, Fraser DJ, Spiegelman GB, Fisher PR, Weeks G, Insall RH (2000). Dictyostelium RasD is required for normal phototaxis, but not differentiation. Genes Dev 14, 1407–1413.
Williams TD, Paschke PI, Kay RR (2019). Function of small GTPases in Dictyostelium macropinocytosis. Philos Trans R Soc Lond B Biol Sci 374, 20180150.
Wu L, Gaskins C, Zhou K, Firtel RA, Devreotes PN (1994). Cloning and targeted mutations of G alpha 7 and G alpha 8, two developmentally regulated G protein alpha-subunit genes in Dictyostelium. Mol Biol Cell 5, 691–702.
Wu L, Valkema R, Van Haastert P, Devreotes P (1995). The G protein β subunit is essential for multiple responses to chemoattractants in Dictyostelium. J Cell Biol 129, 1667–1675.
Xu X, Jin T (2019). ELMO proteins transduce G protein-coupled receptor signal to control reorganization of actin cytoskeleton in chemotaxis of eukaryotic cells. Small GTPases 10, 271–279.
Yan J, Mihaylov V, Xu X, Brzostowski JA, Li H, Liu L, Veenstra TD, Parent CA, Jin T (2012). A Gbetagamma effector, ElmoE, transduces GPCR signaling to the actin network during chemotaxis. Dev Cell 22, 92–103.
Yuen IS, Gomer RH (1994). Cell density-sensing in Dictyostelium by means of the accumulation rate, diffusion coefficient and activity threshold of a protein secreted by starved cells. J Theor Biol 167, 273–282.
Zhang ER, Liu S, Wu LF, Altschuler SJ, Cobb MH (2016). Chemoattractant concentration-dependent tuning of ERK signaling dynamics in migrating neutrophils. Sci Signal 9, ra122.
Zhang S, Charest PG, Firtel RA (2008). Spatiotemporal regulation of Ras activity provides directional sensing. Curr Biol 18, 1587–1593.